New Reduction Factor for Cracked Multi-planar Square Hollow Section TT-, YT- and KT-joints

S.T. Lie, S.P. Vipin* and T. Li

*School of Civil & Environmental Engineering
Nanyang Technological University
50 Nanyang Avenue
Singapore 639798
E-mail: vipin1@e.ntu.edu.sg, Tel.: +65-91403876

ABSTRACT

Many existing multi-planar structures such as bridges, buildings and others are fabricated using square hollow section (SHS) members. There are no guidance's available in the design codes to assess the safety and integrity of these cracked multi-planar SHS joints till date. This paper proposes a new set of equations for determining the reduction factor (F_{AR}) of cracked multi-planar SHS TT-, YT- and KT-joints. A completely new and robust finite element (FE) mesh generator is developed and it is validated using the experimental test results. Parametric study is carried out for multi-planar SHS joints subjected to axial loading at the brace end. The results reveal that the crack area and the brace to chord width ratio (β) have an important effect on the plastic collapse load of the cracked SHS joints. For a particular β value, the F_{AR} varies up to 4.37% for different values of crack area.

Keywords: Finite element analysis; Multi-planar joints; Plastic collapse load; Reduction factor; Surface crack

Nomenclature

a	crack depth
A_c	crack area

b_0	chord width
b_1, b_2	brace width
E	Young's modulus
F_{AR}	reduction factor
g	gap distance
h_0	chord height
h_1, h_2	brace height
l_c	chord length
l_w	weld length
P_c	plastic collapse load
t_0	chord thickness
t_1, t_2	brace thickness
α	chord length to half chord width ratio
β	brace to chord width ratio
γ	chord half width to thickness ratio
τ	brace thickness to chord thickness ratio
θ_1, θ_2	brace to chord angle

1. Introduction

The previous research works conducted on multi-planar tubular joints focus solely on uncracked models [1-5]. Yu et al. [1] observed that the load capacity for uncracked multi-planar rectangular hollow section (RHS) TT-joints at plastic collapse limit is increased by up to 26% more than that of uncracked uni-planar RHS T-joint. However, their work did not vary the geometric parameters such as β and γ, and they recommended that further parametric studies are required to quantify the multi-planar effect of the joints covering the whole range of geometrical parameters. The design resistance or plastic collapse load (P_c) for each relevant plane of an uncracked multi-planar joint is determined by applying an appropriate multi-planar factor to the strength of the corresponding uncracked uni-planar

joint [6]. For the case of cracked multi-planar joints, a reduction factor (F_{AR}) must be used. The F_{AR} when multiplied with the P_c load of uncracked multi-planar SHS joints, gives the P_c load of cracked multi-planar SHS joints.

The F_{AR} equation for uni-planar circular hollow section (CHS) tubular joints proposed by Burdekin et al. [7] has been incorporated in BS7910:2005 [8], Guide to methods for assessing the acceptability of flaws in metallic structures, and is expressed as

$$F_{AR} = \left[1 - \frac{\text{crack area}}{\text{weld length} * \text{chord thickness}}\right]\left[\frac{1}{Q_\beta}\right]^{m_q} \quad (1)$$

where Q_β is the geometrical modifier which depends on brace to chord width ratio (β) values, and it is expressed as

$$Q_\beta = 1, \text{ for } \beta \leq 0.6 \quad (2)$$

$$Q_\beta = \frac{0.3}{[\beta(1-0.833\beta)]}, \text{ for } \beta > 0.6 \quad (3)$$

For tubular joints containing part-thickness flaws, $m_q = 0$ and for tubular joints containing through-thickness flaws, $m_q = 1$. There are two main limitations in using the above equations for cracked multi-planar SHS TT-, YT- and KT-joints. Firstly, the study used to derive F_{AR} shown in equation (1) was carried out on uni-planar CHS joints [7]. So it may not produce optimal solutions for other joints such as cracked multi-planar SHS TT-, YT- and KT-joints. Secondly, it is given in the BS7910:2005 [8] that for CHS tubular joints containing part-thickness flaws (surface cracks), $m_q = 0$. In that case, the $(\frac{1}{Q_\beta})^{m_q}$ term from equation (1) will become one indicating that the 'β' has no effect in the estimation of F_{AR} for cracked CHS

tubular joints. However, the present parametric study shows that the β has an influence on the F_{AR} values for cracked multi-planar SHS TT-, YT- and KT-joints containing surface cracks; the results of which will be described in the subsequent sections. Therefore, the main objective of this paper is to propose a new set of equations for determining the F_{AR} of cracked multi-planar SHS TT-, YT- and KT-joints subjected to axial tensile loading at the brace end. The F_{AR} equations for cracked uni-planar SHS T-joints subjected to axial tensile loading at the brace end are already published by the authors [9].

2. New finite element (FE) mesh generator

The new FE mesh generator for cracked multi-planar SHS TT-, YT- and KT-joints is developed based on some on-going research works in Nanyang Technological University, Singapore [9-18]. Based on the experiment test results [11, 12], the fatigue crack is modelled in the numerical model, and they are introduced at the corner of the weld toe at the hot spot stress location. It is observed that the shape of the crack is not symmetrical. Yang [11] approximated the crack shape as two half semi-elliptical cracks, and therefore, it is also adopted in the present study. The conventional dimensional notations used in the SHS joints are given in Fig. 1 [6, 19].

2.1. Meshing details

A completely new and robust FE mesh generator is developed by the authors to generate meshes automatically for different types of uncracked and cracked SHS joints [9, 16, 17, 18]. The new FE mesh generator uses one type of element .i.e. 20 nodes hexahedral element to model the cracked SHS joints. Different types of elements such as hexahedral elements with 20 nodes, pyramid elements with 20 nodes, Prism elements with 15 nodes and

tetrahedron elements with 10 nodes were used in previous study [11]. The usage of different types of elements resulted in generation of elements with very sharp angles. Therefore, the convergence of solutions is not achieved whenever large strain values are involved.

Another drawback of the previous study is the early termination of FE analysis especially for very large deformation [11]. This tendency was predominantly observed for elastic-plastic analyses during the calculation of *J*-integral. The elements at the crack tip are observed to collapse during elastic-plastic analyses and therefore, appropriate convergence of solutions is not achieved. The new FE mesh generator addresses this issue by using a key-hole for the modelling the crack tip used in elastic-plastic analyses. In general, there are two methods to construct crack tip elements for elastic-plastic analyses. Fig. 2.a shows the first method where the crack tip nodes are coincident and untied. This method results in the development of crack tip blunting due to large strains formed during the analyses. If the deformation at the crack is relatively small, it can still generate accurate elastic-plastic *J*-integral (J_{ep}) results [17]. However, if the deformation is very large, the crack tip elements may collapse, producing invalid elastic-plastic *J*-integral (J_{ep}) results. For a very large plastic deformation, it is frequently encountered that the solution cannot converge. In order to overcome this difficulty, Anderson [20] recommended using a key-hole, shown in Fig. 2.b, having a finite radius within the plastic zone at the crack tip. Therefore, crack tip elements having a finite radius key-hole are adopted in the present study. This helps greatly in avoiding the elements enclosing the crack tip from collapsing and ensuring convergence even at a very large plastic deformation. The selection of finite radius needs to be carefully chosen. If the finite radius is too small, the elements around the crack tip may still collapse, while if the finite radius is too large, it may affect the accuracy of the results because the finite radius of key-hole should lie

within the plastic zone [12]. The value of key-hole radius is adopted in accordance with the recommendations given in API RP579 [21], i.e. it should be at least five times smaller than tip radius in the deformed state. In the new FE mesh generator, the finite radius of the key-hole is set as a variable so that an appropriate value can be chosen by the users. It was observed that the value of 0.1mm is sufficient to accommodate the large scale non-linear deformation at the crack tip without the collapsing of elements. So from the current research study, the authors recommend a range for key-hole radius form 0.05 to 0.15 with 0.1 as the most desirable value for load values in the range of 1000 kN.

One another major limitation of the previous approach relates to the overall mesh design approach used for cracked SHS models [11]. The crack block is inserted into the previously generated uncracked SHS model. The border segments of the inserted crack block should exactly coincide with the mesh of uncracked SHS models. This requirement restricts the crack end position or in other words, the mesh generator is not flexible enough to account for cracks with varying lengths. In the new FE mesh generator, crack block is embedded in the SHS model. Separate FE mesh models are created for both uncracked and cracked SHS joints. The new FE mesh generator is versatile enough to account for cracks of any arbitrary length and is also flexible for modelling various combinations of unsymmetrical cracks having different depths. The “spider web” configuration which is the most efficient mesh design for the crack tip region enables a smooth conversion from a fine mesh to a coarser mesh away from the high stress concentration region. Mesh refinement and zoning techniques are extensively used in the new FE mesh generator so that it is robust to model different types of uni-planar and multi-planar SHS welded joints with and without cracks.

The basic sequence to form the brace part of a SHS T-joint is illustrated in Fig. 3. The crack tube, transition zone and crack block of a flat plate are modelled first. Transition zones are then used to connect the crack tube with the other parts of the structure. Thereafter, adjacent mesh zones of the flat plate are modelled. Subsequently, the flat plate is converted to T-butt geometry by adding weld attachments. In this study, mapping techniques are used to transform 2-D crack front of the parent T-butt geometry into 3-D crack front of the SHS joints. Finally, the remaining parts of brace and chord are generated to complete the modelling of SHS joints. Figs. 4 to 6 show the completed mesh of cracked multi-planar SHS TT-, YT- and KT-joints, respectively.

2.2. Experimental validation of new FE mesh generator

Full-scale SHS T-, Y- and K-joints experimental tests had previously been tested to failures in the industry sponsored project completed by the authors [11, 12]. The above mentioned experimental test results are used to check the validity and accuracy of the new FE mesh generator. A specifically designed test rig shown in Fig. 7 is used to test the cracked SHS T-joints. The rig comprises of two servo-hydraulic actuators which can produce ±1000 kN load and ±125 mm displacement capacity respectively. The loads are applied to the two ends of the spread beam by the actuators. Subsequently, the loads are transferred to the brace end via the 6 bolts stiffened to the spread beam as depicted in Fig. 8. As a result, a total maximum axial load of 2000 kN can be applied to the specimen. Instron 8500 controller is used to control the actuators. The controller can be set either in load control or in displacement control. Regarding the support condition at both chord ends, pinned end condition were created by using a pin and a roller placed on top of 600 mm × 600 mm concrete supports as illustrated in Fig. 8.

For SHS Y- and K-joints, another test rig was used for the static tests as shown in Fig. 9. The ends of the chord were fixed with the yellow rig as shown in Figs. 10(a) and 10(b) for Y- and K-joints respectively. Two hydraulic jackets were used to apply the loads on the end of the brace. Each hydraulic jacket can produce 1000 kN load capacity.

Figs. 11 to 13 represent the load-displacement curves obtained from experimental test results as well as numerical results using the new FE mesh generator. The load-displacement curves for SHS T-, Y- and K-joints clearly reveal the analogous trends between experimental and numerical models. Hence, the numerical models created using the new FE mesh generator are accurate and slightly un-conservative, and it can be used to carry out extensive parametric study of cracked SHS T-, Y- and K-joints. Further extensive numerical validation of the new FE mesh generator can also be found in other published works reported by the authors [9, 16, 17, 18].

3. Parametric study

The various codes of practises recommend a correction factor to uni-planar joint strength which is equivalent to the P_c load to determine the P_c load of corresponding uncracked multi-planar SHS joints [6, 19, 23]. As mentioned before, when F_{AR} is multiplied with the P_c load of uncracked multi-planar SHS joints, gives the P_c load of cracked SHS joints. The equations for determining the P_c load of uncracked multi-planar SHS joints takes into consideration of the effect of β, and hence, due importance is given for the same in the current parametric study. The next critical parameter to be considered in the parametric study is crack area factor. The crack area factor represents the percentage of crack area with respect to the total cross-sectional area. From equation (1), it can be seen that the total cross-

sectional area is obtained by multiplying total weld length with the chord thickness. For example, a crack area factor of 10% indicates that the value of $\left(\frac{\text{crack area}}{\text{weld length} * \text{chord thickness}} \right) * 100\,\%$ is equal to 10%.

3.1. Geometry and material properties

The details of various geometries used in the parametric study are given in Table 1. 11 different values of β are analyzed for crack area values of 5.8%, 10%, 20% and 0%. The dimensions of the new multi-planar brace such as the length and width of the brace as well as the weld details are kept the same as the brace of uni-planar joints. The brace thickness to chord thickness ratio (τ) is kept constant throughout the parametric study. The thickness for the brace and chord used is 16.0 mm. All the chord length to half chord width ratio (α) values used in the parametric study are above 8.0 so that the effect of α on estimating the P_c load of multi-planar SHS TT-, YT- and KT-joints is eliminated [24].

The material used in the present study for cracked multi-planar SHS TT-, YT- and KT-joints is BS4360 structural steel of grade 50D, and the stress-strain curve of the material is shown in Fig. 14. The axial tensile loads are applied at the brace ends using displacement control. In the FE analyses, the new FE mesh generator produce the input files (models) automatically, which are then analysed using the commercial ABAQUS software [25]. In ABAQUS, loading can be either applied through load-control or displacement control. The present study uses displacement control. Gradually increasing displacement values are applied to the brace end, which are equivalent to applying gradually increasing load values. Finally, the load-displacement curves are obtained for each model and subsequent calculations are carried out. The Young's modulus and Poisson's ratio of the material used are 210 kN/mm^2

and 0.3, respectively. Regarding the boundary conditions, the nodes at the brace end where the axial loading is applied is set free. And all the chord ends and non-loaded brace ends are pinned (Fig. 15). For all the cases used in the present study, the chord length is kept at a constant value of 3000 mm. A long value of chord length ensures that the effect of chord end boundary conditions on the failure of damaged joints is negligible [11].

4. Results and discussion

In the present study, the twice-elastic compliance (TEC) criterion is used to determine the deformation limits. Past studies have used the TEC criterion to determine the P_c load of cracked tubular joints [17, 26, 27]. This plastic criterion is defined in ASME VIII Division 2 [28] as the twice-elastic slope (TES) criterion. The TEC criterion is established on the load-deformation response of a structure in the plastic analysis as shown in Fig. 16. The P_c load is the load corresponding to the intersection of the load-deformation curve and the twice elastic compliance line. The twice elastic compliance line start from the origin of the load-deformation curve and has twice the slope of the initial elastic response [17], which is obtained using the equation

$$\tan\varphi = 2\tan\theta \tag{4}$$

where φ and θ are the angles measured from the load axis as shown in Fig. 16.

The comparison of numerical model with the real fractured sample is illustrated in Fig. 17. It is clearly observed that the failure mode for both the cases is punching shear. The FE mesh model of a typical multi-planar SHS TT-joint used in the parametric study is depicted in Fig. 18. The shape of model before and after the analysis is illustrated, and it can be observed that a considerable yielding has occurred particularly around the brace-chord intersection which

is the high stress concentration region. The load-displacement curves for the multi-planar SHS TT-joints are represented in Figs. 19 to 21. Brace end axial loading values are plotted against brace end displacement for crack area values of 5.8%, 10% and 20%. In the curves, results from lower and higher β values are plotted, and it is observed that the P_c load of the multi-planar SHS TT-joints joints increases with increasing value of β. Similar variation is observed for the load versus displacement curves for SHS YT- and KT-joints, and hence, they are not shown in this paper.

4.1. Effect of brace to chord width ratio (β)

Using the FE analyses results, the load-displacement relationship of the SHS TT-, YT- and KT-joints are plotted to obtain the P_c load. The reduction factor (F_{AR}) is calculated using the following expression,

$$F_{AR} = \frac{\text{Plastic collapse load of cracked SHS joint}}{\text{Plastic collapse load of uncracked SHS joint}} \tag{5}$$

Similar to the observation made for cracked uni-planar SHS joints [9], the present study shows that β has an influence on F_{AR} for cracked multi-planar SHS TT-, YT- and KT-joints (Figs. 22 to 24). For a particular value of crack area, F_{AR} vary from 0.31% to 2.71% for different values of β. It is observed that the influence of β value in F_{AR} estimation for multi-planar joints is less when compared to uni-planar joints. In other words, F_{AR} obtained for multi-planar joints are higher when compared to the same for uni-planar joints. This is expected since the presence of an additional brace in multi-planar joints increases the P_c load, and thereby, increasing the stiffness of the brace-chord intersection zone in multi-planar joints. For low brace to chord width ratio (β) value, the failure mode observed is

punching shear, and it is observed for a β value up to 0.50. In the case of higher β values, the failure mode observed is chord face plastification. In chord face plastification failure mode, extensive bending of the chord face is observed.

4.2. Effect of crack area factor

The reduction factor (F_{AR}) is primarily introduced to account for the reduction in P_c load due to the presence of cracks in tubular joints. Therefore, the crack area has the most significant influence on F_{AR} of cracked multi-planar SHS TT-, YT- and KT-joints. Figs. 25, 27 and 29 depict the variation in the F_{AR} with the crack area for punching shear failure mode; while Figs. 26, 28 and 30 depict the same for chord face plastification failure mode. The parametric study reveals that for cracked multi-planar SHS joints, F_{AR} varies from 1.52% to 4.37% for different values of crack area. For the uni-planar SHS joints, the variation range from is 1.9% to 5.3% [9]. Generally, it is observed that F_{AR} decreases with an increase in crack area value. As the crack size increases, the P_c load of the cracked multi-planar SHS TT-, YT- and KT-joints decreases, thereby, weakening the strength of joints. Therefore, a lower value of F_{AR} which is calculated as per equation (5) is obtained.

The parametric study shows that the F_{AR} decreases to 4.37% in the case of cracked multi-planar SHS TT- and YT-joints and 4.15% in the case of cracked multi-planar SHS KT-joints for crack area of 20%. It is worth to mention the above smaller percentage reduction value for KT-joints relative to TT- and YT-joints. The presence of an additional brace in KT-joints increases the local stiffness of the joint, and thereby, increasing the bearing capacity to withstand the effect of cracks.

4.3. Proposed equations for reduction factor (F_{AR})

It is clear from the Sub-sections 4.1 and 4.2 that F_{AR} vary non-linearly with β and crack area for SHS TT-, YT- and KT-joints. This non-linear variation necessitates the use of non-linear regression techniques to curve fit the numerical data obtained from the parametric study. Hence, for the two failure modes observed for cracked multi-planar SHS TT-, YT- and KT-joints, two set of equations are proposed after carrying out the non-linear regression.

The proposed equations for TT- and YT-joints are as follows:

$$\text{For } \beta \geq 0.5;\ F_{AR} = \left(1 - \frac{A_c}{l_w * t_0}\right)^{0.23} * \beta^{0.01} * 1.02 \tag{6}$$

$$\text{For } \beta < 0.5;\ F_{AR} = \left(1 - \frac{A_c}{l_w * t_0}\right)^{0.11} * \beta^{-0.02} * 0.98 \tag{7}$$

The proposed equations for KT-joints are as follows:

$$\text{For } \beta \geq 0.5;\ F_{AR} = \left(1 - \frac{A_c}{l_w * t_0}\right)^{0.22} * \beta^{0.01} * 1.01 \tag{8}$$

$$\text{For } \beta < 0.5;\ F_{AR} = \left(1 - \frac{A_c}{l_w * t_0}\right)^{0.10} * \beta^{-0.02} * 0.98 \tag{9}$$

where A_c is the crack area, l_w is the weld length and t_0 is the chord thickness.

The coefficient of determination values for TT- and YT- joints are 0.957 and 0.903, and for

KT-joints are 0.959 and 0.912. These high values for the non-linear regression justify the statistical accuracy of the proposed equations. For verifying the proposed equations further, the reduction factor (F_{AR}) values from the numerical data and the F_{AR} values obtained from the regression equations are plotted and compared as shown in Figs. 31 to 36. The plots reconfirm the accuracy of the proposed regression equations as the values for both the considered cases exhibit good agreement.

5. Conclusions

Plastic collapse analyses of cracked multi-planar SHS TT-, YT- and KT-joints are performed for the first time in the present study. It can be observed clearly that the stress at the brace-chord intersection corner is the highest compared to the other regions of the SHS TT-, YT- and KT-joints. The reduction factor (F_{AR}) obtained for multi-planar joints are higher when compared to the same for uni-planar joints due to the presence of an additional brace which increases the P_c load, and thereby, increasing the stiffness of the brace-chord intersection zone in multi-planar joints. For a particular value of crack area, F_{AR} vary from 0.31% to 2.71% for different values of β. The crack area has the most significant influence on F_{AR} of cracked multi-planar SHS TT-, YT- and KT-joints. The study reveals that the F_{AR} decreases to 4.37% in the case of cracked multi-planar SHS TT- and YT-joints and 4.15% in the case of cracked multi-planar SHS KT-joints for crack area of 20%. Non-linear regression techniques are used to curve fit the numerical data obtained from the parametric study and a new set of equations for F_{AR} of cracked multi-planar SHS TT-, YT- and KT-joints are proposed. The F_{AR} values from the numerical data and the regression equations are plotted and compared. The plots reconfirm the accuracy of the proposed regression equations as the

values for both the considered cases exhibit good agreement

Acknowledgements

The authors would like to thank Maritime Research Centre in the School of Civil and Environmental Engineering at Nanyang Technological University, Singapore, and Maritime Port Authority of Singapore for funding this research project under the Grant No. MPA 23/04.15.03 – RDP 005/06/031.

References

[1] Yu Y, Liu DK, Puthli RS, Wardenier J. Numerical Investigation into Static Behaviour of Multi-Planar Welded T-joints in RHS. Tubular structures V. Proc. 5th Int symposium on tubular structures, Nottingham, UK 1993;732–48.

[2] O'Connor MA. Static Strength of Multi-planar K-joints in Rectangular Hollow Sections: Numerical Modelling. Tubular structures V. Proc. 5th Int symposium on tubular structures, Nottingham, UK 1993;749–56.

[3] Shahi EP, Puthli RS, Wardenier J. Stress Concentration Factors in KK-Multiplanar Joints Made of Square Hollow Sections Including Welds. Tubular structures V. Proc. 5th Int symposium on tubular structures, Nottingham, UK 1993;529–42.

[4] Herion S, Mang F, Bucak O. Design Proposal for Multiplanar K-joints with Gap Made of Rectangular Hollow Sections. Tubular structures VI. Proc. 6th Int symposium on tubular structures, Melbourne, Australia 1994;551–59.

[5] Lee MMK, Wilmshurst SR. Numerical Modelling of CHS Joints with Multiplanar Double-K Configuration. J Constr Steel Res 1995;32:281-301.

[6] Packer JA, Wardenier J, Zhao XL, van der Vegte GJ, Kurobane Y. Design Guide for rectangular hollow section (RHS) joints under predominantly static loading. 2nd ed.

CIDECT 3, Geneva,Switzzerland, 2009.

[7] Burdekin FM, Thurlbeck SD, Cowling MJ. Defect assessment in offshore structures application of BSI document PD 6493:1991. Proc. 11th Int Conf Offshore Mech Arctic Engng, Calgary, Canada 1992;411–19.

[8] BS7910-Amendment 1. Guide to methods for assessing the acceptability of flaws in metallic structures, British Standards Institution, UK, 2005.

[9] Lie ST, Vipin SP, Li T. New Reduction Factor for Cracked Square Hollow Section T-joints under Axial Loading. J Constr Steel Res 2015; 112:221-27.

[10] Lie ST, Li G, Cen Z. Analysis of cracked tubular joints using coupled finite and boundary element methods. Eng Struct 2000; 22:272–83.

[11] Yang ZM. Ultimate strength and fracture behaviour of cracked welded square hollow section T-Joints. Ph.D. thesis, Nanyang Technological University, Singapore, 2005.

[12] Lie ST, Chiew SP, Lee CK, Yang ZM. Static strength of cracked square hollow section T joints under axial loads. I: experimental. J Struct Engng 2006; 132:368–77.

[13] Chiew SP, Lee CK, Lie ST, Ji HL. Fatigue Behaviour of Square-to-Square Hollow Section T-Joint with Corner Crack. I: Experimental studies. Engng Fract Mech 2007; 74:703–20.

[14] Lee CK, Chiew SP, Lie ST, Sopha T. Comparison of fatigue performances of gapped and partially overlapped CHS *K*-joints. Eng Struct 2011; 33:44–52.

[15] Lie ST, Yang ZM. Plastic collapse load of cracked square hollow section T-, Y-, and K-joints. J. Offshore Mech.Arct. Eng. 2011; 133:1-10.

[16] Lie ST, Vipin SP, Li T. A new mesh modelling technique for elastic-plastic analyses of cracked plate- to- plate and circular hollow section welded joints. Proc. 11th Int

Conf Steel Space Composite Structures, Qingdao, China 2012;259–68.

[17] Lie ST, Li T, Shao YB. Plastic collapse load prediction and failure assessment diagram analysis of cracked circular hollow section T-joint and Y-joint. Fatigue Fract Eng Mater Struct 2014;37:314–24.

[18] Lie ST, Vipin SP, Li T. New Weld Toe Magnification Factors for Semi-Elliptical Cracks in Double-Sided T-butt Joints and Cruciform X-Joints. Int J of Fatigue 2015; 80:178-91.

[19] IIW. Static design procedure for welded hollow section joints – recommendations. Int Inst of Welding, IIW Doc. XV-1329-09, IIW Doc. XV-E-09-400, 2005.

[20] Anderson TL. Fracture Mechanics, Fundamentals and Applications, 3rd ed., CRC Press, Boston, USA, 2005.

[21] API RP579. Fitness-for-Service, American Petroleum Institute, Washington, USA, 2007.

[22] FEACrack™, User's Manual, Version 3.2, Quest Integrity Group LLC., USA, 2010.

[23] Eurocode 3: design of steel structures-part 1-8: design of joints, British Standard Institute, UK, 2005.

[24] Stacey A, Sharp JV, Nichols NW. The influence of cracks on the static strength of tubular joints. Proc. 15th Int Conf Offshore Mech Arctic Engng, Florence, Italy 1996;435–50.

[25] ABAQUS. Standard user's manual, Version 6.11, Hibbett, Karlsson & Sorensen, Inc., USA, 2011.

[26] Stacey A, Sharp JV, Nichols NW. Static strength assessment of cracked tubular joints. Proc. 15th Int Conf Offshore Mech Arctic Engng, Florence, Italy 1996;211–

24.

[27] Muscat M, Mackenzie D, Hamilton R. A Work Criterion for Plastic Collapse. Int J Pres Piping 2003; 80:49-58.

[28] ASME VIII Division 2. Rules for construction of pressure vessels. American Society of Mechanical Engineers,USA,1998.

Table 1

Dimensions of specimens for crack area of 5.8%, 10%, 20 % and 0%

b_1	b_2	t_0	t_1	l_c	β	b_0	γ	α	τ
150.0	150.0	16	16	3000	0.25	600.0	18.8	10.0	1
150.0	150.0	16	16	3000	0.30	500.0	15.6	12.0	1
150.0	150.0	16	16	3000	0.35	428.6	13.4	14.0	1
150.0	150.0	16	16	3000	0.40	375.0	11.7	16.0	1
150.0	150.0	16	16	3000	0.45	333.3	10.4	18.0	1
150.0	150.0	16	16	3000	0.50	300.0	9.4	20.0	1
150.0	150.0	16	16	3000	0.55	272.7	8.5	22.0	1
150.0	150.0	16	16	3000	0.60	250.0	7.8	24.0	1
150.0	150.0	16	16	3000	0.65	230.8	7.2	26.0	1
150.0	150.0	16	16	3000	0.70	214.3	6.7	28.0	1
150.0	150.0	16	16	3000	0.75	200.0	6.3	30.0	1

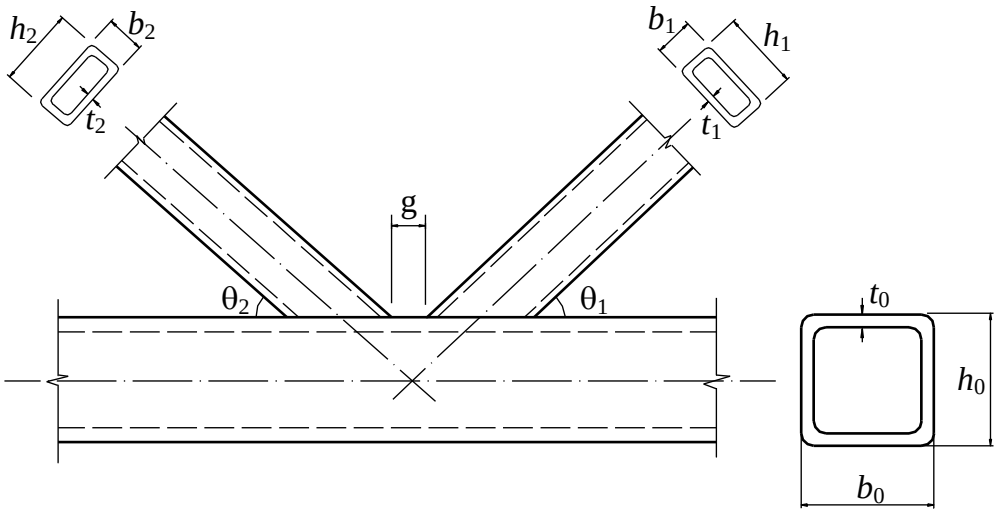

Fig. 1 Dimensional notations used by CIDECT [6] and IIW [19]

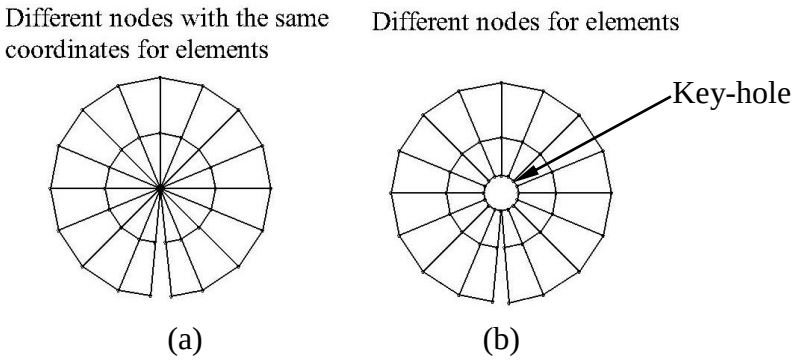

Fig. 2 Different methods used to model the crack tip for elastic-plastic analyses

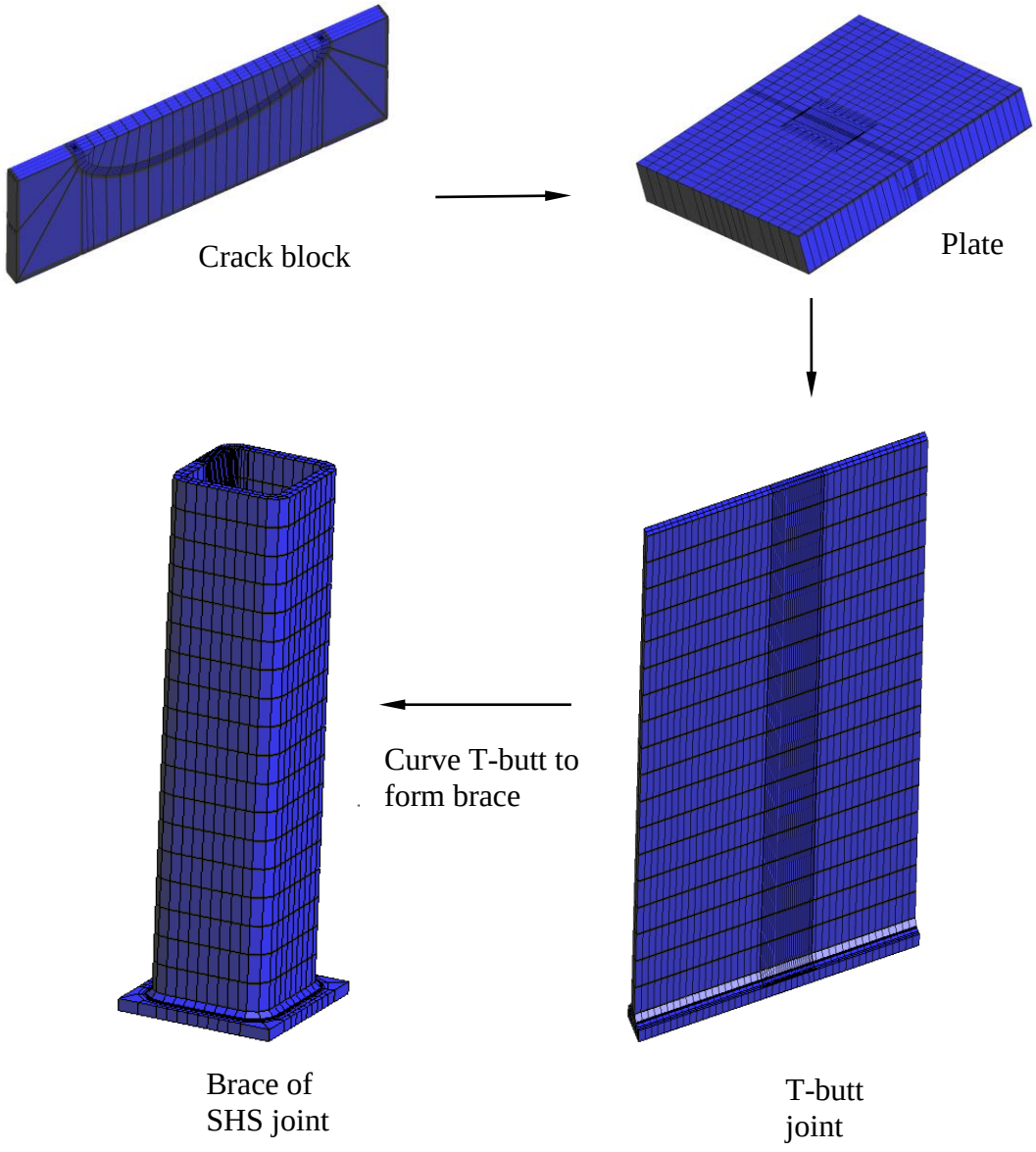

Fig. 3 Sequence to form the main brace of SHS T-joint

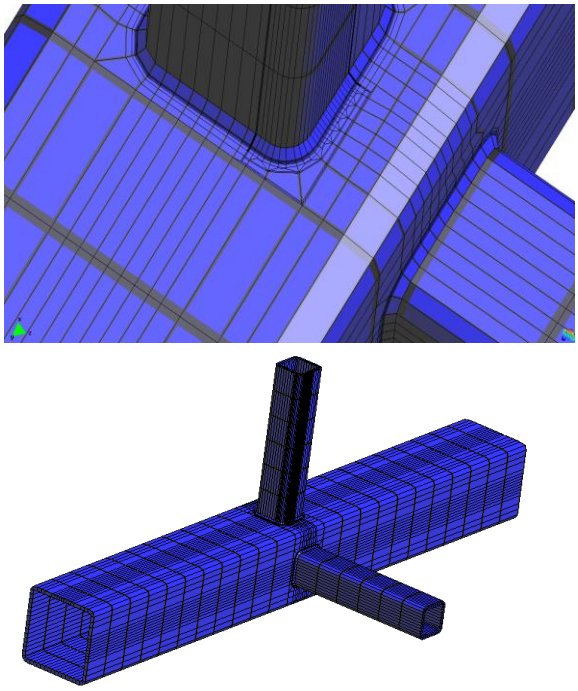

Fig. 4 The completed mesh of a cracked multi-planar SHS TT-joint

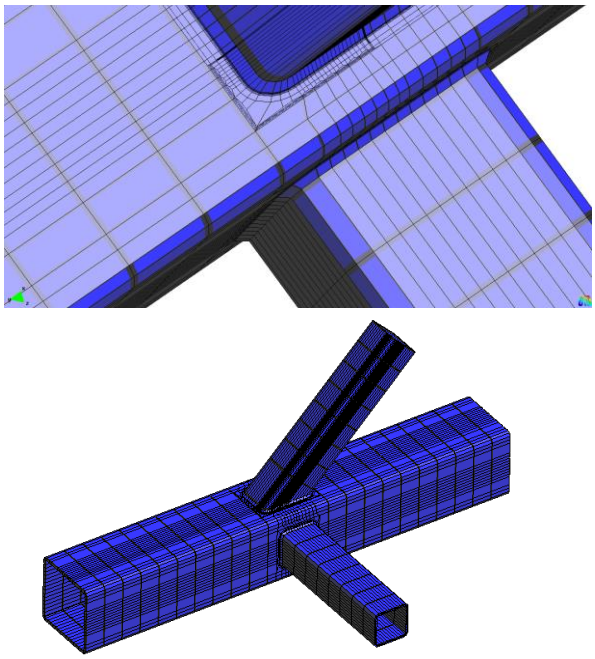

Fig. 5 The completed mesh of a cracked multi-planar SHS YT-joint

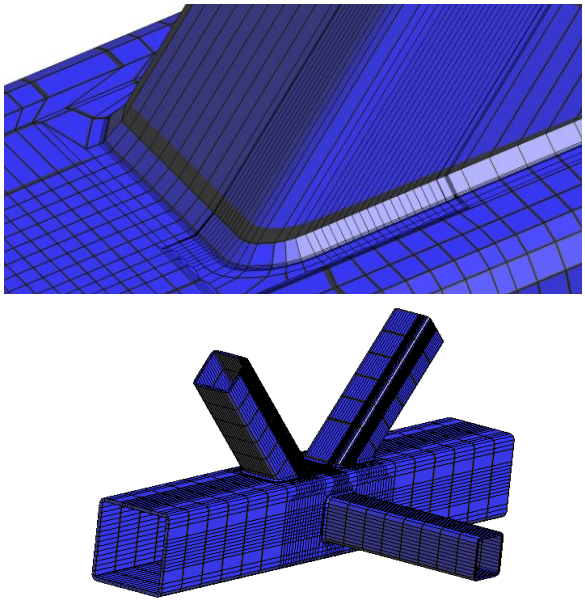

Fig. 6 The completed mesh of a cracked multi-planar SHS KT-joint

Fig. 7 Test rig for SHS T-joint [11]

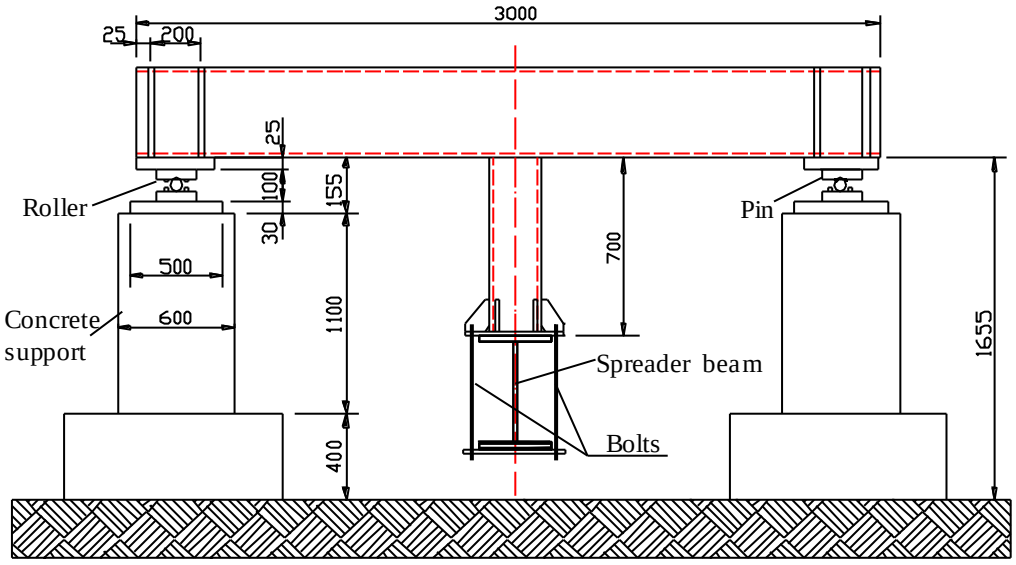

Fig. 8 Setup of the experimental test [11]

Fig. 9 Test rig used to test the Y- and K-joints [11]

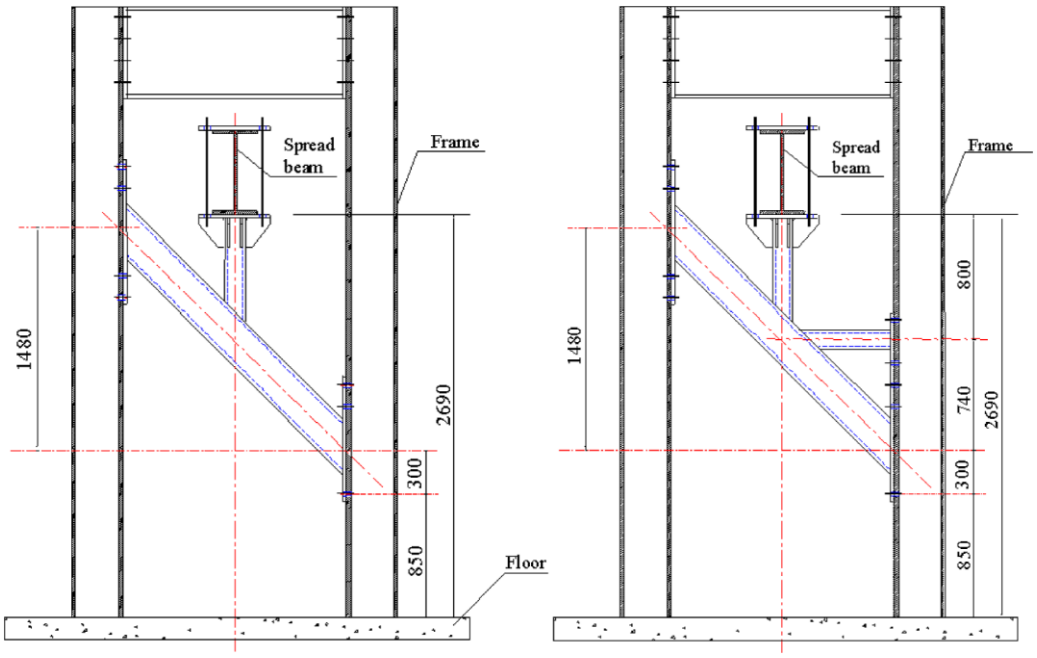

(a) (b)

Fig. 10 Schematic view of the test rig used to test the Y- and K-joints [11]

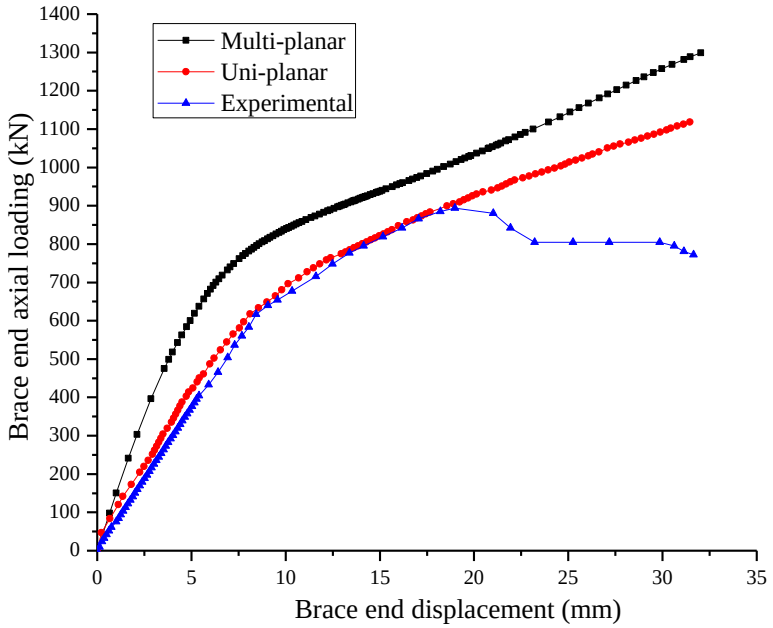

Fig. 11 Comparison of load-displacement curves of uni-planar and multi-planar SHS T-joints

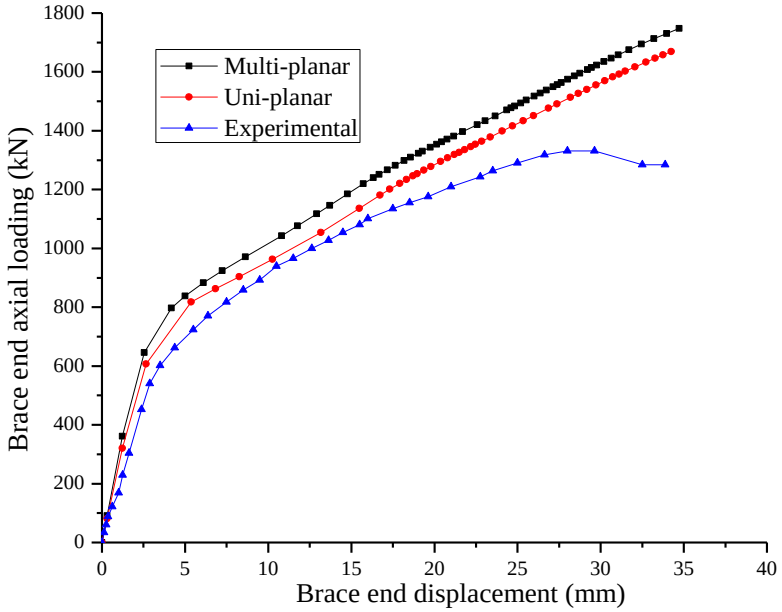

Fig. 12 Comparison of load-displacement curves of uni-planar and multi-planar SHS Y-joints

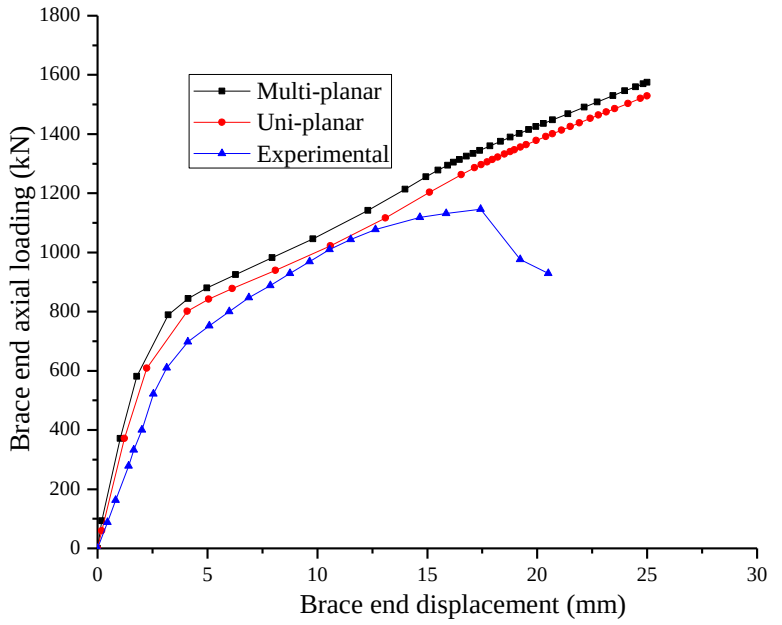

Fig. 13 Comparison of load-displacement curves of uni-planar and multi-planar SHS K-joints

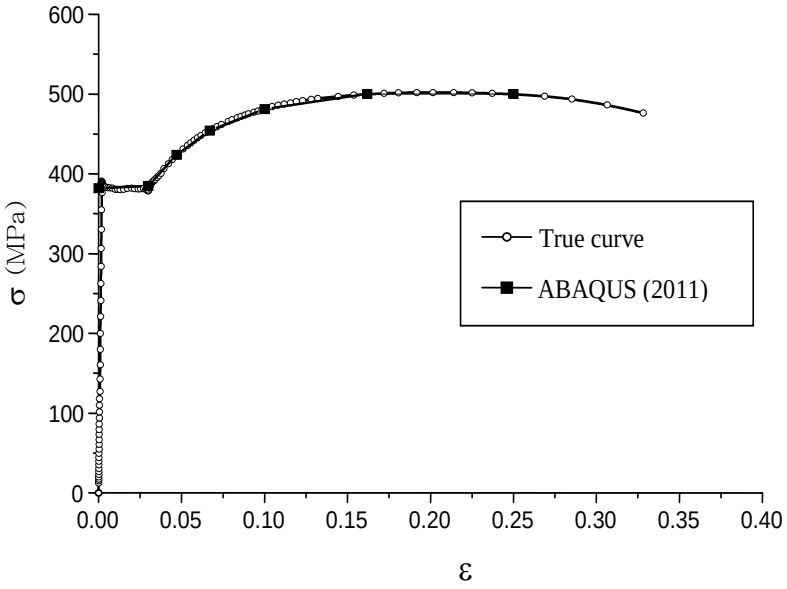

Fig. 14 Stress-strain curve of the BS4360-50D structural steel

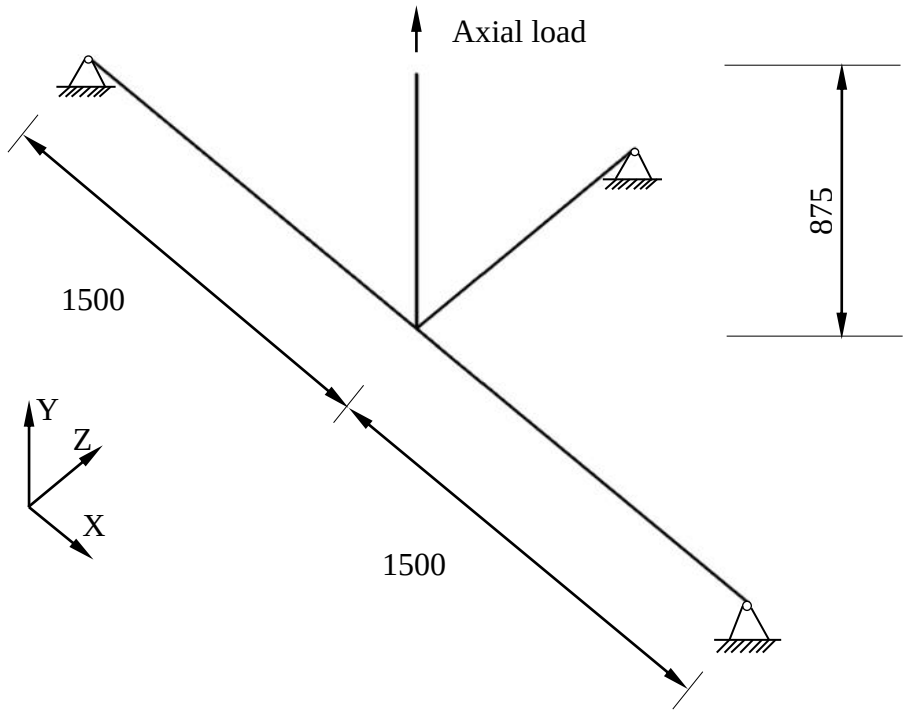

Fig. 15 Loading and boundary conditions

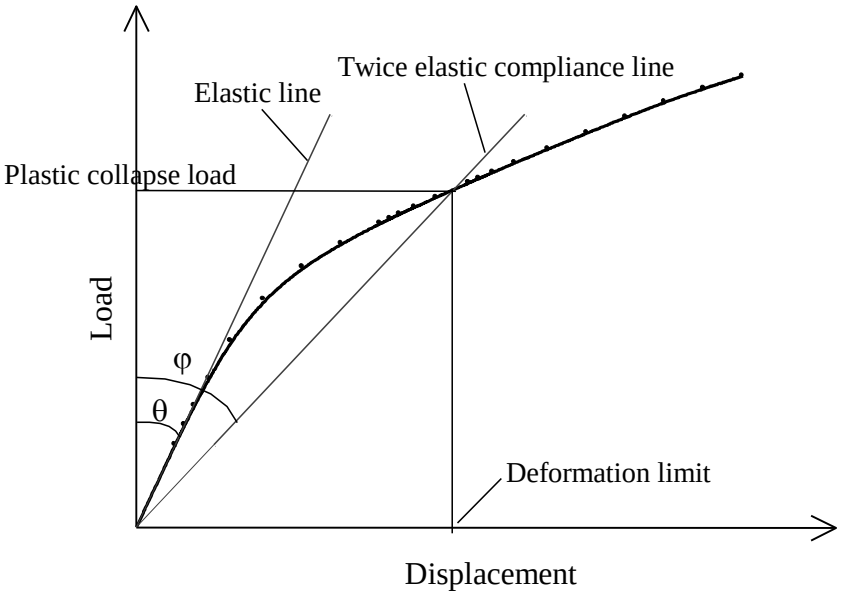

Fig. 16 Twice elastic compliance criterion

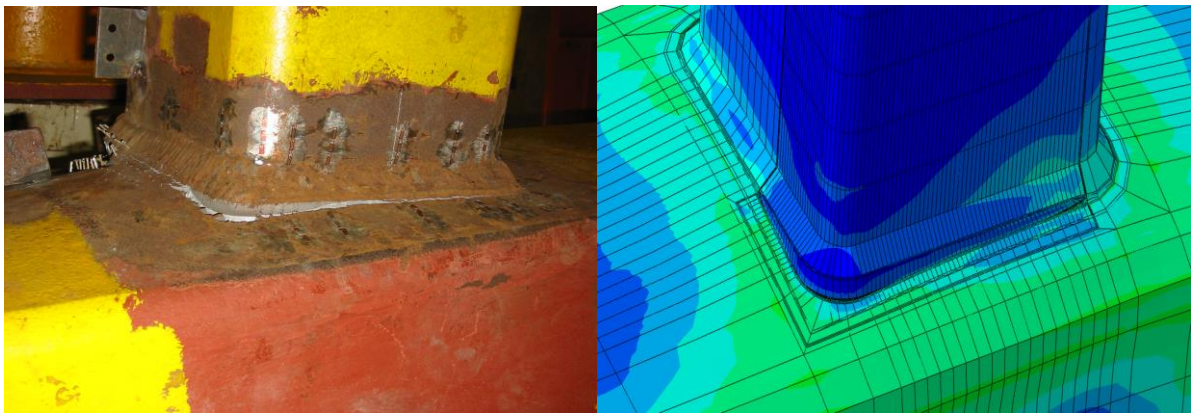

Fig. 17 Comparison with real fractured sample

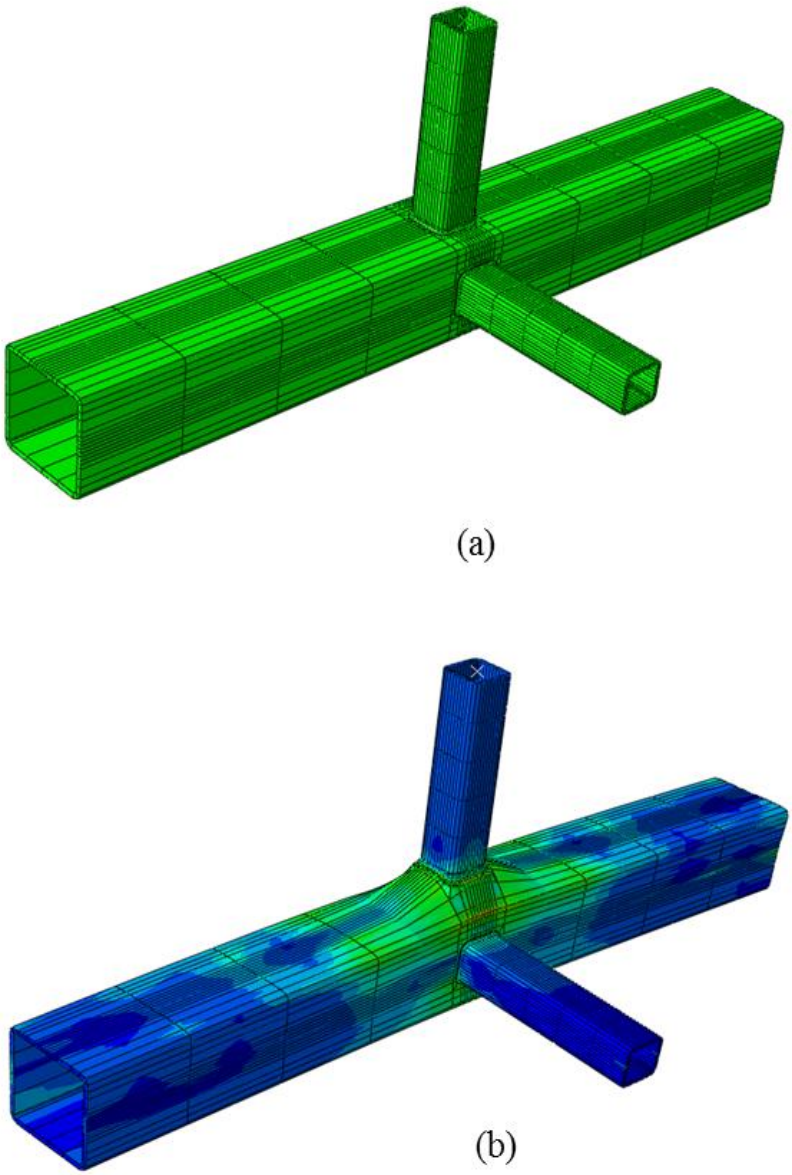

Fig. 18 Typical multi-planar SHS models: (a) before FE analysis; (b) after FE analysis, with deformation plotted using a scale of 1.5:1

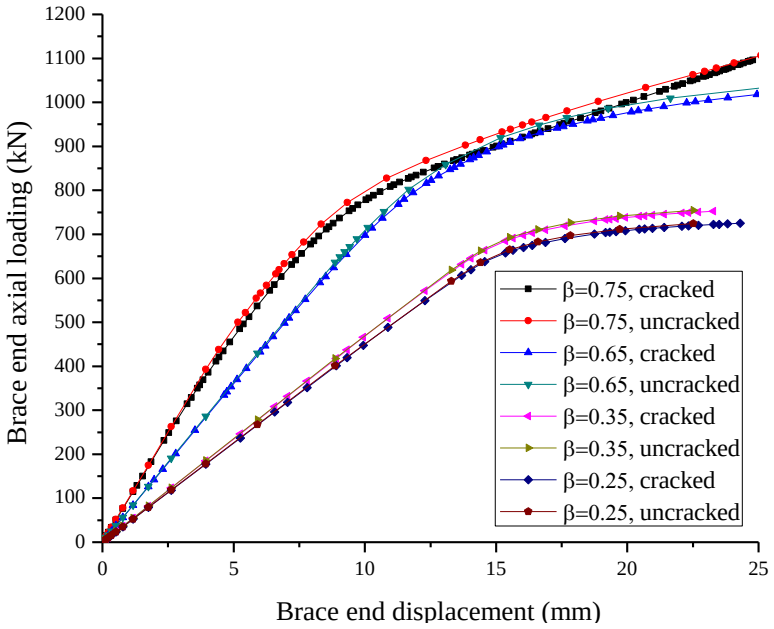

Fig. 19 Load vs displacement curve for crack area 5.8% for multi-planar TT-joints

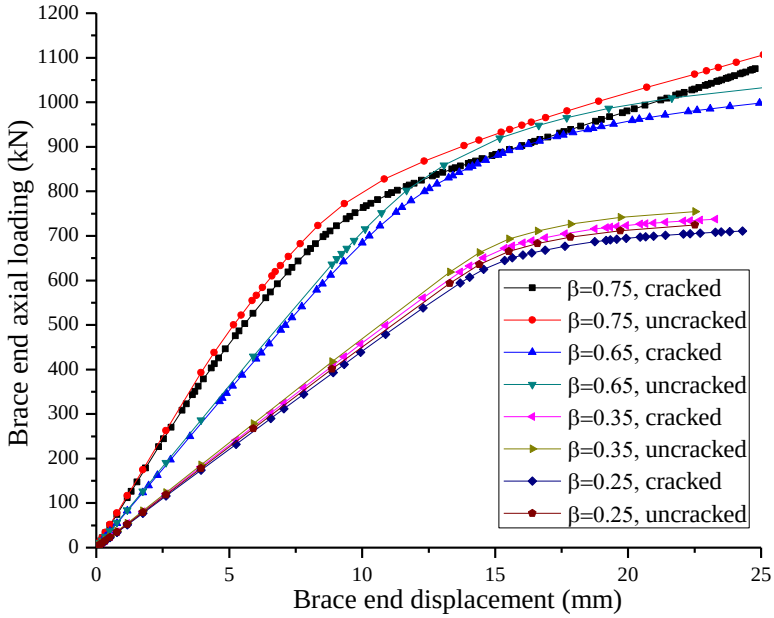

Fig. 20 Load vs displacement curve for crack area 10% for multi-planar TT-joints

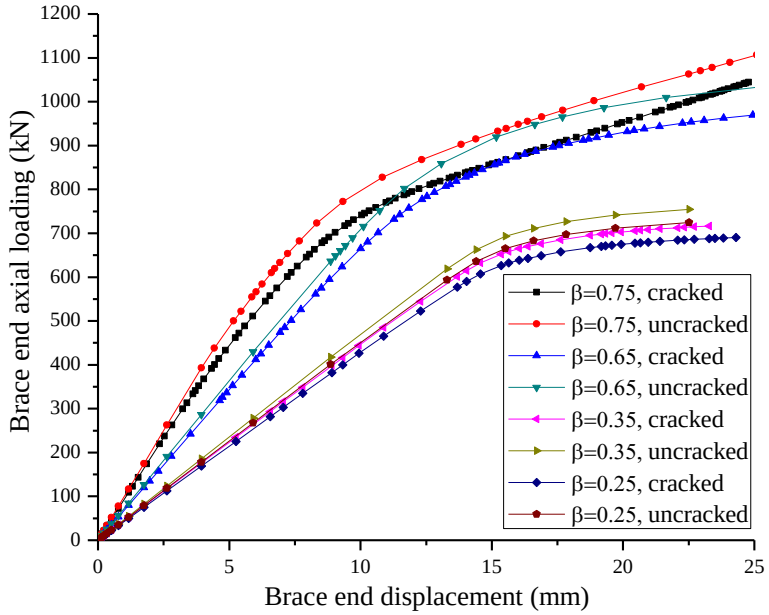

Fig. 21 Load vs displacement curve for crack area 20% for multi-planar TT-joints

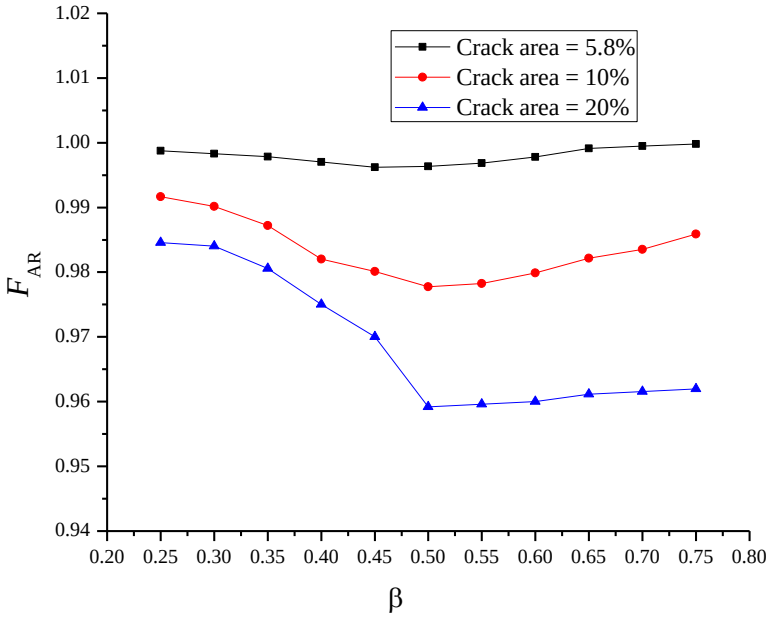

Fig. 22 F_{AR} vs β plot comparison for multi-planar SHS TT-joints

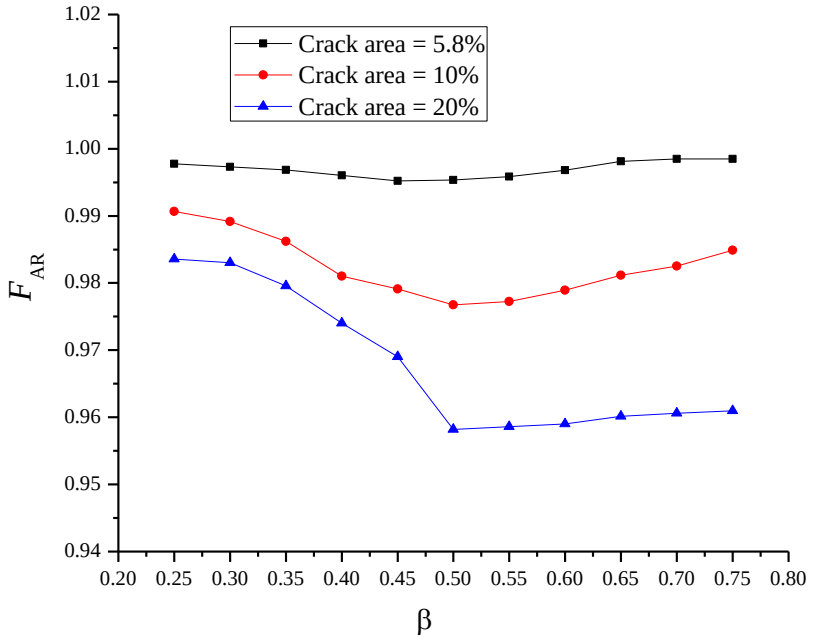

Fig. 23 F_{AR} vs β plot comparison for multi-planar SHS YT-joints

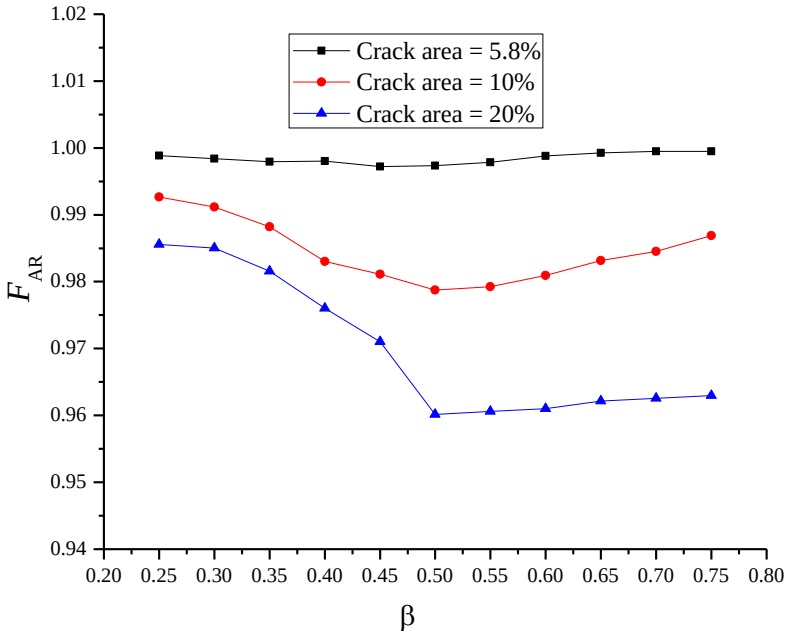

Fig. 24 F_{AR} vs β plot comparison for multi-planar SHS KT-joints

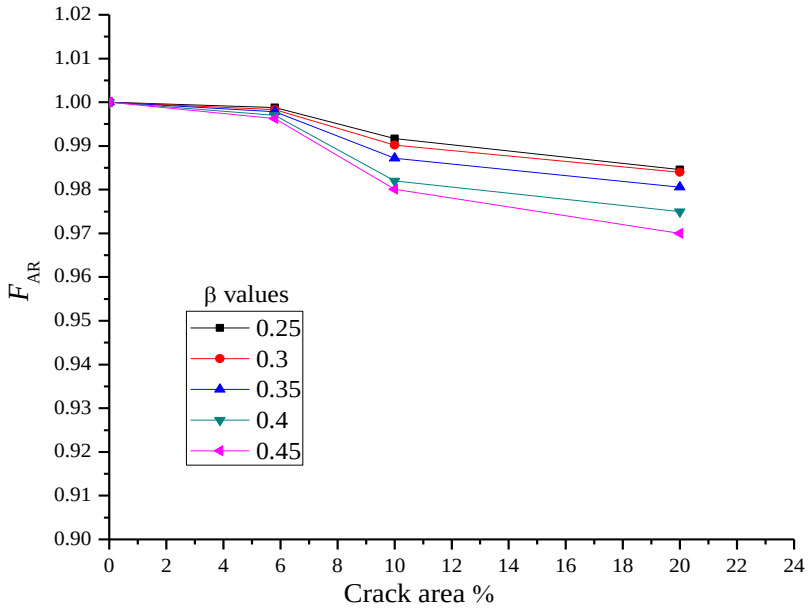

Fig. 25 Comparison of F_{AR} vs crack area plot of multi-planar SHS TT-joints for β<0.5

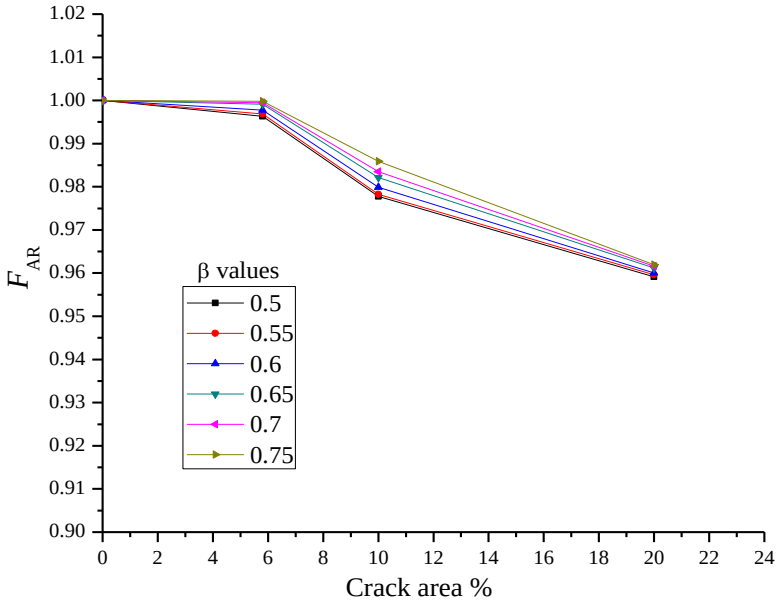

Fig. 26 Comparison of F_{AR} vs crack area plot of multi-planar SHS TT-joints for β≥0.5

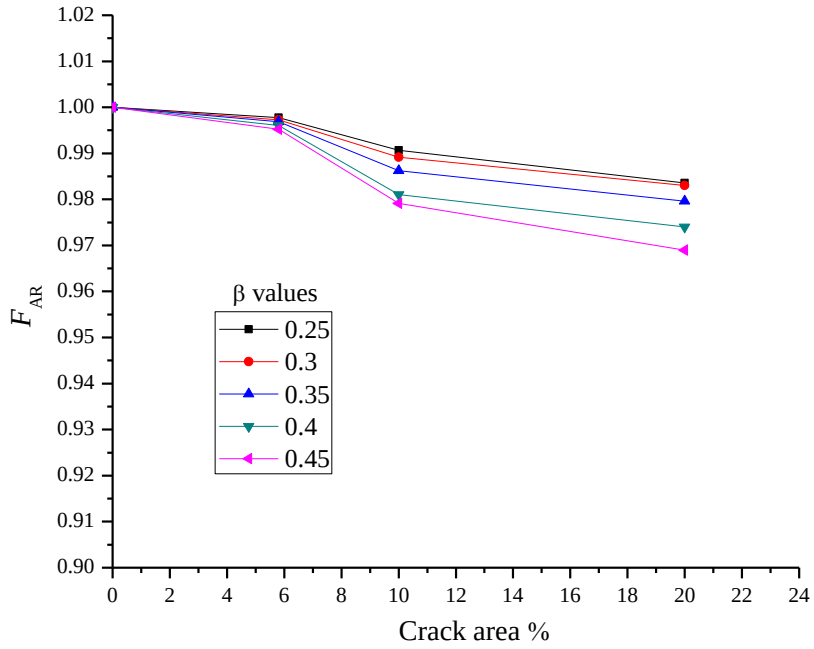

Fig. 27 Comparison of F_{AR} vs crack area plot of multi-planar SHS YT-joints for β<0.5

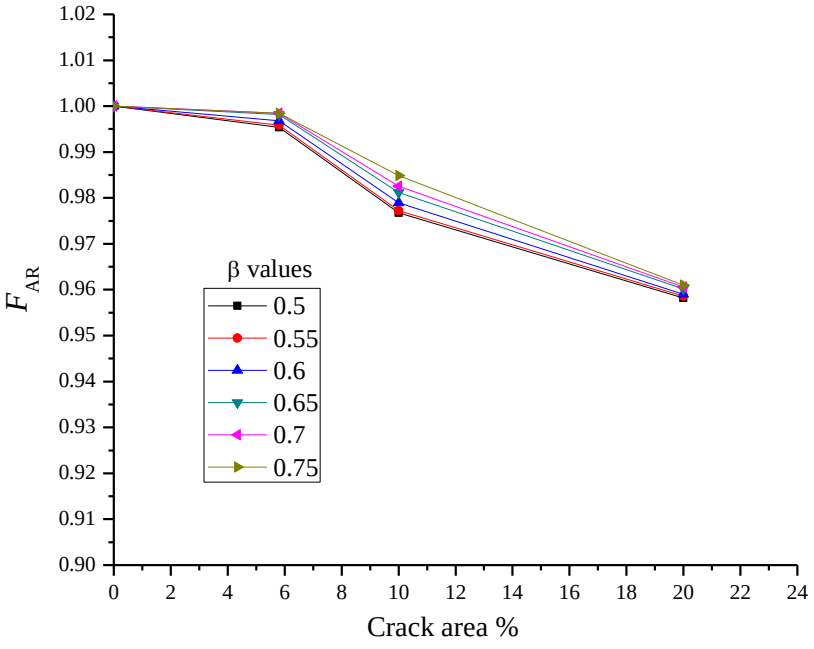

Fig. 28 Comparison of F_{AR} vs crack area plot of multi-planar SHS YT-joints for β≥0.5

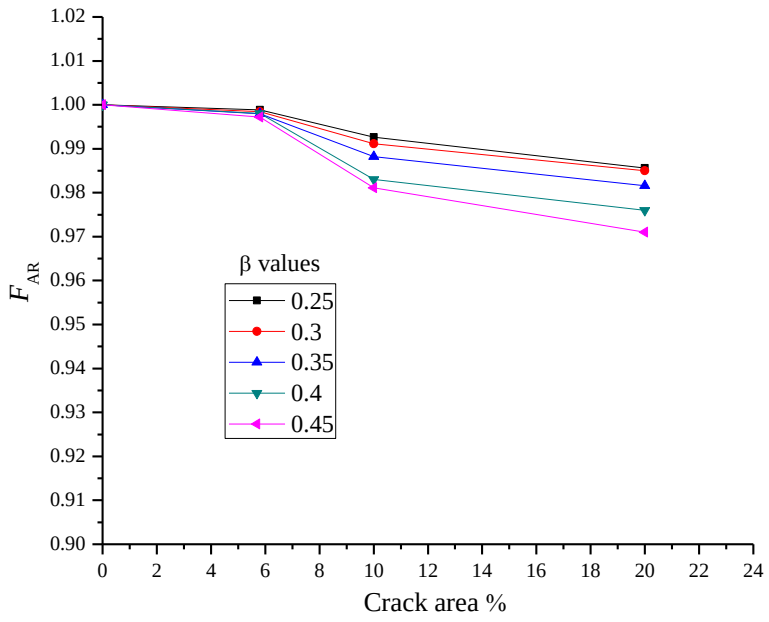

Fig. 29 Comparison of F_{AR} vs crack area plot of multi-planar SHS KT-joints for β<0.5

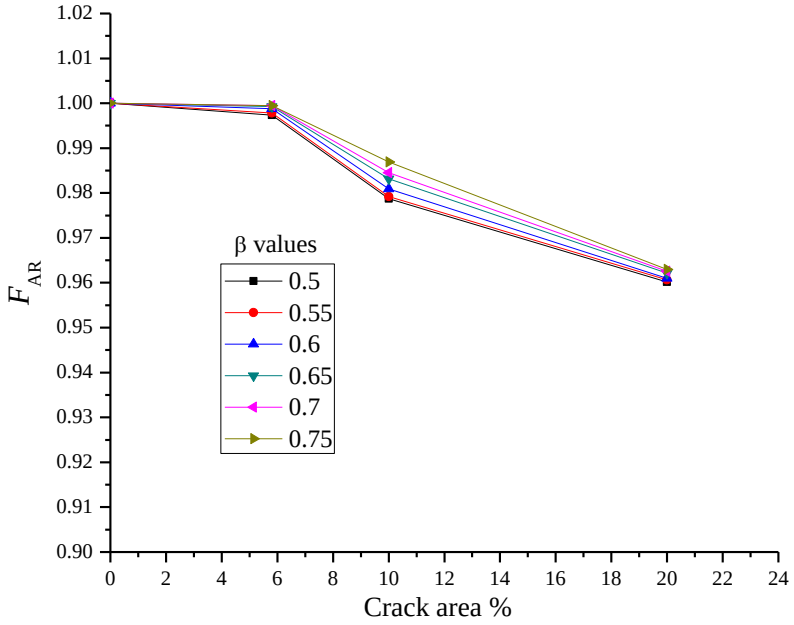

Fig. 30 Comparison of F_{AR} vs crack area plot of multi-planar SHS KT-joints for β≥0.5

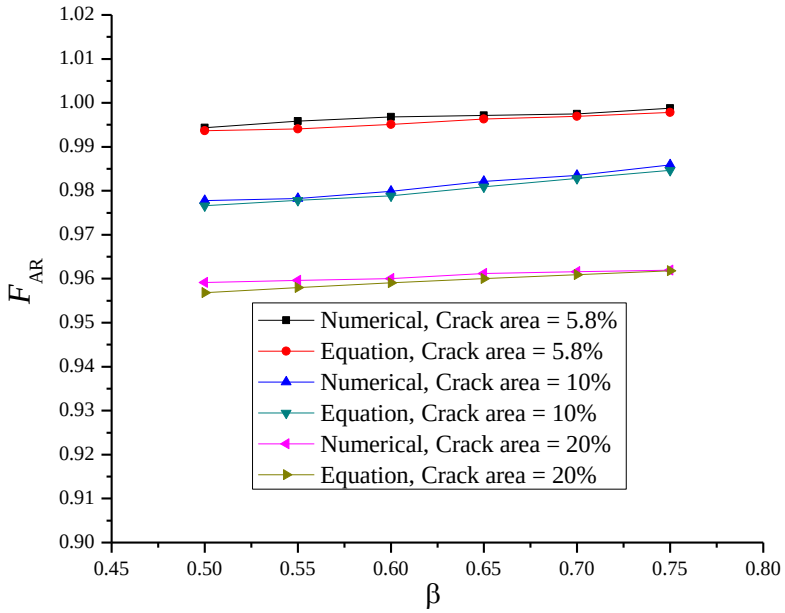

Fig. 31 Comparison of equation predictions with the numerical data for multi-planar SHS TT-joints for β≥0.5

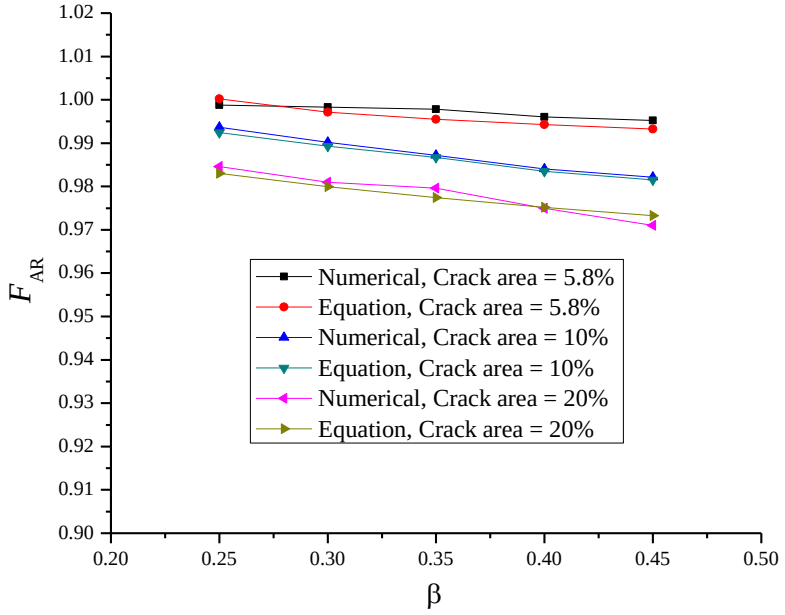

Fig. 32 Comparison of equation predictions with the numerical data for multi-planar SHS TT-joints for β<0.5

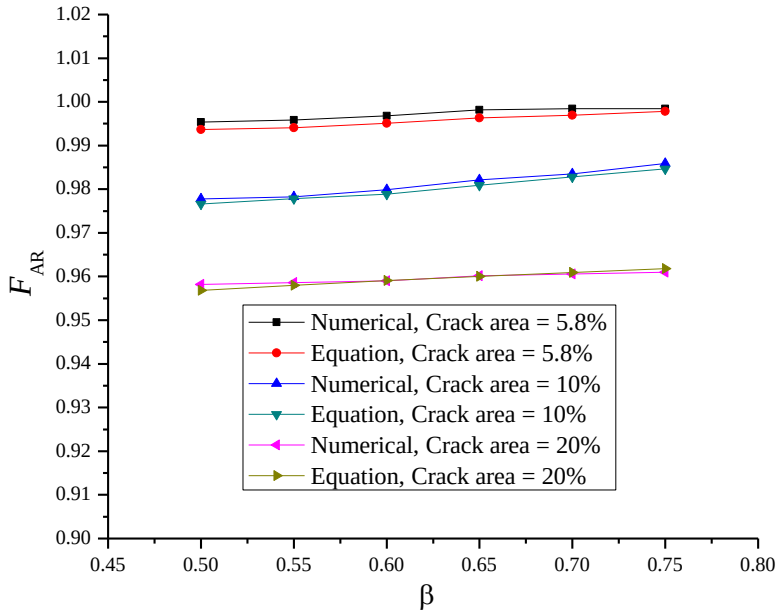

Fig. 33 Comparison of equation predictions with the numerical data for multi-planar SHS YT-joints for β≥0.5

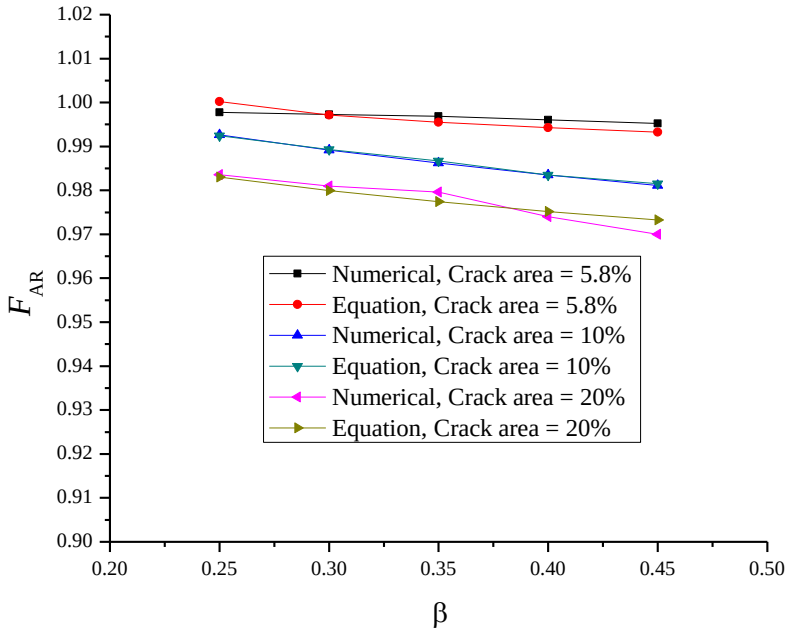

Fig. 34 Comparison of equation predictions with the numerical data for multi-planar SHS YT-joints for β<0.5

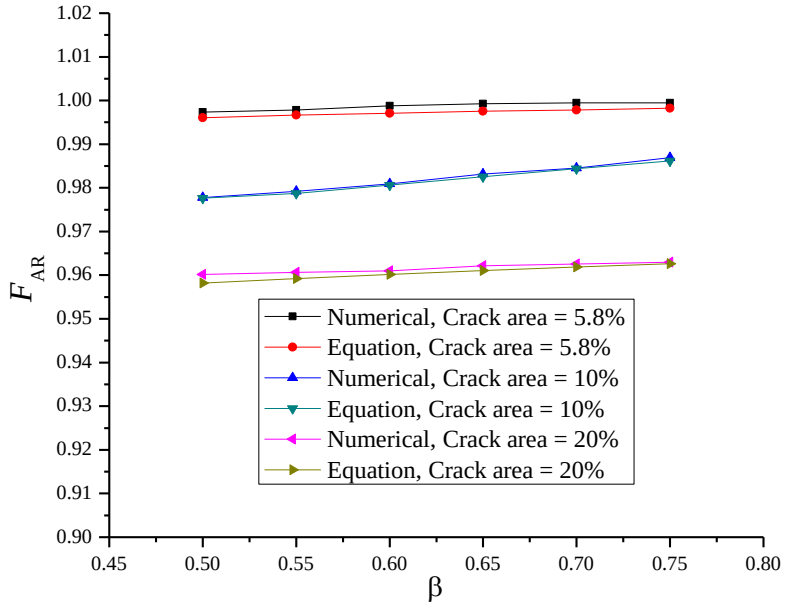

Fig. 35 Comparison of equation predictions with the numerical data for multi-planar SHS KT-joints for β≥0.5

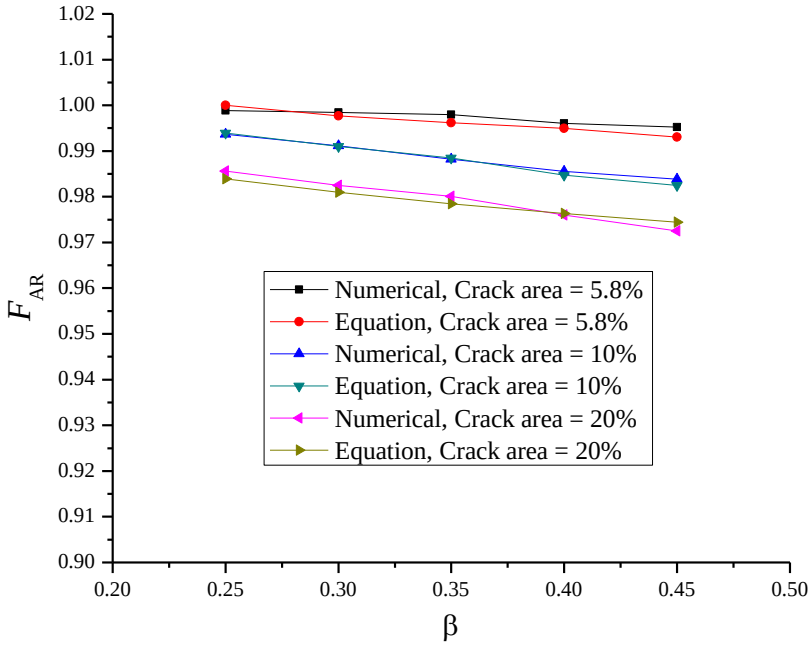

Fig. 36 Comparison of equation predictions with the numerical data for multi-planar SHS KT-joints for β<0.5